Supplementary Material for "Microfluidic Salt Precipitation: Implications for Geological CO_2 Storage"

Tsai-Hsing Martin Ho[1] and Peichun Amy Tsai[1,†]

[1] *Department of Mechanical Engineering,*

University of Alberta, Edmonton, Alberta, Canada T6G 2G8

Abstract

In this Supplementary Information, we firstly detail the microfluidic patterns used for our (quasi-) 2D porous network with two different porosity values: $\phi = 0.52$ and $\phi = 0.23$. The unit pore space used for each porosity case is described. Secondly, we describe the microfabrication processes, including the standard deep reactive ion etching (DRIE) and replica molding steps. Thirdly, we present the methods of post-image analysis of extracting the data of the areas of residual brine and salt crystals from the raw images as well as the calibration of such image analysis. Fourthly, a supporting video is provided, illustrating the dynamics and directions of brine drying and salt precipitation. Finally, we show the results of all the experiments involved in this study.

[†] Corresponding author: peichun.amy.tsai@ualberta.ca

1. PATTERNS OF MICROFLUIDIC POROUS MEDIA

Shown in Fig. S1 are the two microfluidic network patterns used, primarily consisting of regular micro-pillars of a constant height arranged in a 2D ordered lattice. For the case of ϕ = 0.52 in (a), cylindrical micro-pillars align in a body-centered packing of a pillar diameter of d_1 (= 550 μm). The closest distance between two pillars, L_{p1} (= $500\sqrt{2}$ μm). The right image in (a) shows the unit pore area used here, corresponding to the purple area of $A_{p1} = L_{p1}^2 - \pi d_1^2/4 = 2.62 \times 10^5$ μm^2. In (b), for ϕ = 0.23 micro-pillars align in the form of a hexagonal packing, where the pillar diameter $d_2 = 460$ μm. The closest distance between the two pillars is L_{p2} (= 500 μm). The length scales of the pillar diameter and pore throat chosen align with those of Alberta Cambrian Basal Sandstone [1] (medium sand [2]). The unit pore area used for ϕ = 0.23 is shown in the right image of (b), where is $A_{p2} = \left(\sqrt{3}L_{p2}^2/4 - \pi d_2^2/8\right)$ $= 2.51 \times 10^4$ μm^2.

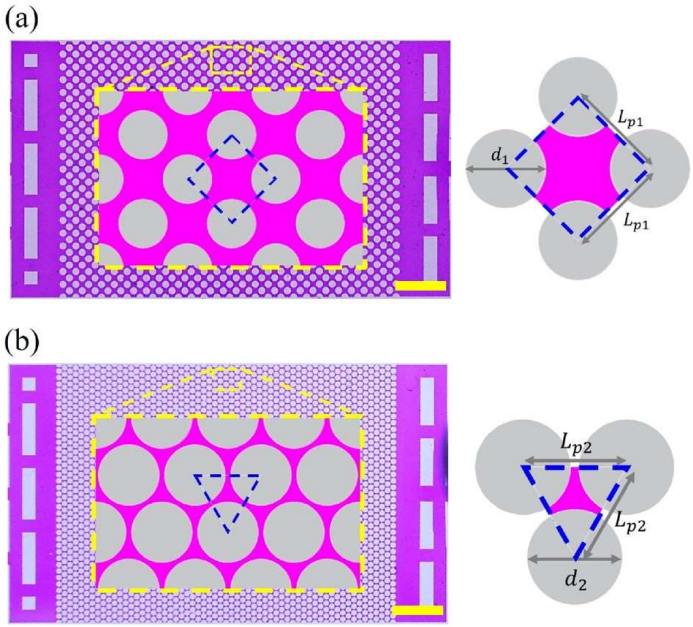

FIG. S1 The patterns of microfluidic porous structures and the schematic of the unit pore area used, for two different porosity (ϕ) values: (a) ϕ = 0.52; (b) ϕ =0.23. The scale bar here presents 4 mm.

2. MICRO-FABRICATION PROCEDURES

A. PROCEDURE OF STANDARD DEEP REACTIVE ION ETCHING (DRIE)

In Fig. S2(a) we summarize the procedure of fabricating the microfluidic mold as a template for making the subsequent PDMS microstructures. First, we dip research-grade silicon wafers into a piranha bath (H_2SO_4:H_2O_2=3:1) for 15 minutes to remove organic residues on the substrates. The cleaned wafers are transferred into the HMDS prime oven (Yield Engineering Systems, Inc.) for the deposition of HMDS (hexamethyldisilazane) for 30 minutes. This HMDS layer acts as the adhesion promoter that helps the subsequent coating of photoresist on the surface uniformly. We spin-coat a thin layer ($2.5\mu m$) of the positive photoresist (HPR 506, FUJIFILM Electronic Materials) on the wafers. The coated wafers are placed to a mask aligner machine (ABM-USA, Inc) together with the photo-mask for exposing under UV light for 3.7 seconds. After the UV exposure, wafers are washed in a photoresist developer bath immediately for at least 90 seconds to remove the uncured photoresist and form the pattern on the wafer surface. To create the desired designs on the silicon surface, we etch the wafers in the inductively coupled plasma reactive-ion etching machine (ICP-RIE, Oxford Estrelas, DSE) [3]. The cured photoresist pattern will protect the silicone surface from bombardment by high energy-intensity plasma. The unprotected area of the wafer surface is etched to the designated depth (about $25\mu m$) and forms the molding patterns. The etched wafers are baked in a plasma etcher (3000 Barrel Etcher, Branson) and soaked in a piranha bath to clean the residual photoresist thoroughly. The result of this fabrication procedure shows in Fig. S2(c).

B. PROCEDURE OF REPLICA MOLDING

Fig. S2(b) shows the steps followed for replica molding. The silicon mold template is first cleaned by DI water and ethanol. After applying the well-mixed PDMS (SYLGARD 184, Dow Corning, 10:1 ratio of silicone elastomer to a curing agent) onto the micro-structured wafers, the entire mold including un-cured PDMS is degassed in a vacuum chamber (for 45 minutes) to remove the bubbles in the PDMS. Subsequently, they were baked in an oven at $60°C$ for an hour to cure the PDMS [4]. After carefully de-molding the cured elastomer from the template, the micro-structured PDMS is bonded to a microscope glass slide by using

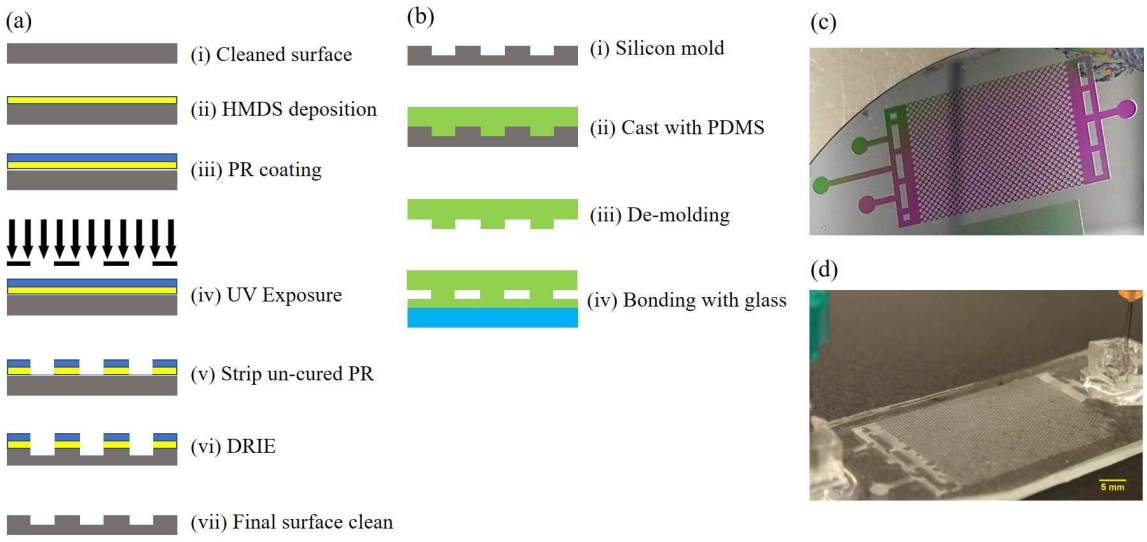

FIG. S2 (a) Process steps used for the micro-fabrication; (b) Replica molding steps using PDMS; (c) Photo of silicon template for the replica-molding method (before final cleaning); (d) A snapshot of the 2D porous PDMS microfluidics.

a high-frequency plasma generator (Electro-Technic Inc., BD-20). The whole assembly is baked in an oven again at $60°C$ for an hour to bind the PDMS and the glass slide firmly. The final PDMS microfluidics is shown in Fig. S2(d).

3. DETAILS OF IMAGE ANALYSIS

A. POST-IMAGE PROCESSES

Fig. S3 is an example of isolating salt nucleation and the residual brine from the raw images to the binary images by thresholding in the CIELAB space. The CIELAB color space measures the brightness change of image from completely dark ($L^* = 0$) to white ($L^* = 100$) (The ImageJ-Fiji linearly expresses the maximum value of L^* to 255 for a RGB image [5]). The color channel a^* represents the components from green ($a^* = 0$) to color red ($a^* = 255$), and the b^* represents from color blue ($b^* = 0$) to yellow ($b^* = 255$) [6]. After several tests, we found that the color space range of $100 < L^* < 104$, $140 < a^* < 150$, and $b^* = 255$ can isolate the salt nucleation from the raw images, as shown in (a). To extract the signal of residual brine, the range of color space is tested to be $100 < L^* < 104$, $140 < a^* < 255$, and $b^* = 255$, as (b) represents. The color channel a^* represents the components from green ($a^* = 0$) to

color red (a^* = 255), and the b^* represents from color blue (b^* = 0) to yellow (b^* = 255).

B. CALIBRATION

We checked and calibrated the processed images with the original raw images against the design parameters. As shown in Fig S3 (c), the diameter of a pillar on the top image, D_r, is measured manually from the raw images. In each case, we manually measured the diameter of ten pillars from the raw images. The average value of D_r has about 2% of the relative error to the design value. The pillar diameter measured from the processed images (D_b) has an additional 1% of relative error on average. Consequently, the maximum accumulative error, resulting from the fabrication and post-image processes, is about 3% in our experiments. We further examine the measurement results of salt nucleation by overlapping the raw data with the binary images. Some salt deposits are not detected by the threshold steps, as shown in Fig. S4. We manually crop these regions and measure the cover area of undetected salt. It is estimated to take about 1.53 % of total salt nucleation on average for the experiments with ϕ = 0.52 porous patterns, while ≈ 3.12% error of undetected salt on average for the ϕ = 0.23 structure.

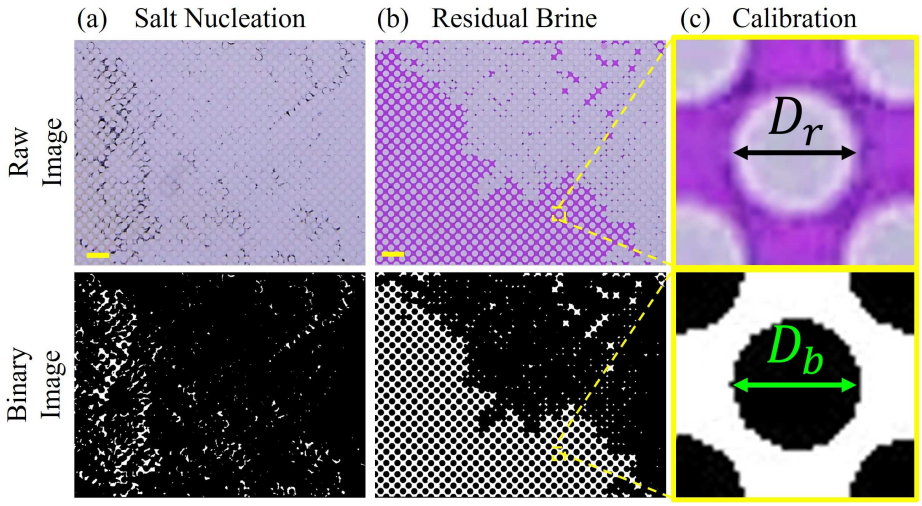

FIG. S3 Post image process for extracting the signals of salt crystals and residual brine from the raw images (represented by the first row of the images) for (a) Salt nucleation and (b) Residual brine. (c) shows a calibration of the raw and the binary images.

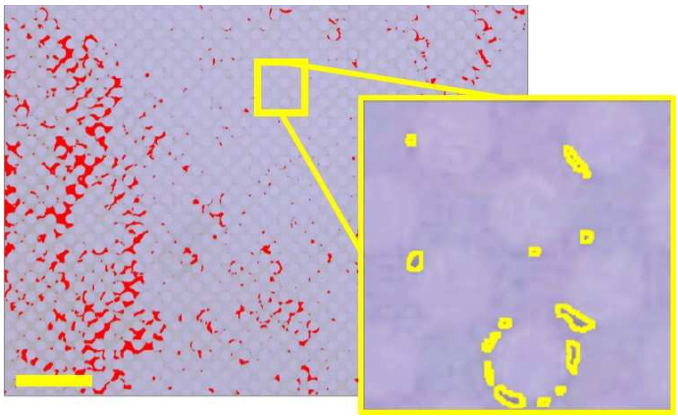

FIG. S4 The isolated salt nucleation (red area) and the undetected salt (spots cropped by yellow lines) after the threshold steps. The scale bar presents 4 mm.

4. SUPPORTING MOVIE

A supporting movie of Fig. 5 in the paper is provided, showing the development of local salt precipitation in the rapid growth regime. It also demonstrates the transportation of salt ions from the residual brine pools to the precipitation front.

5. EXPERIMENTAL DATA

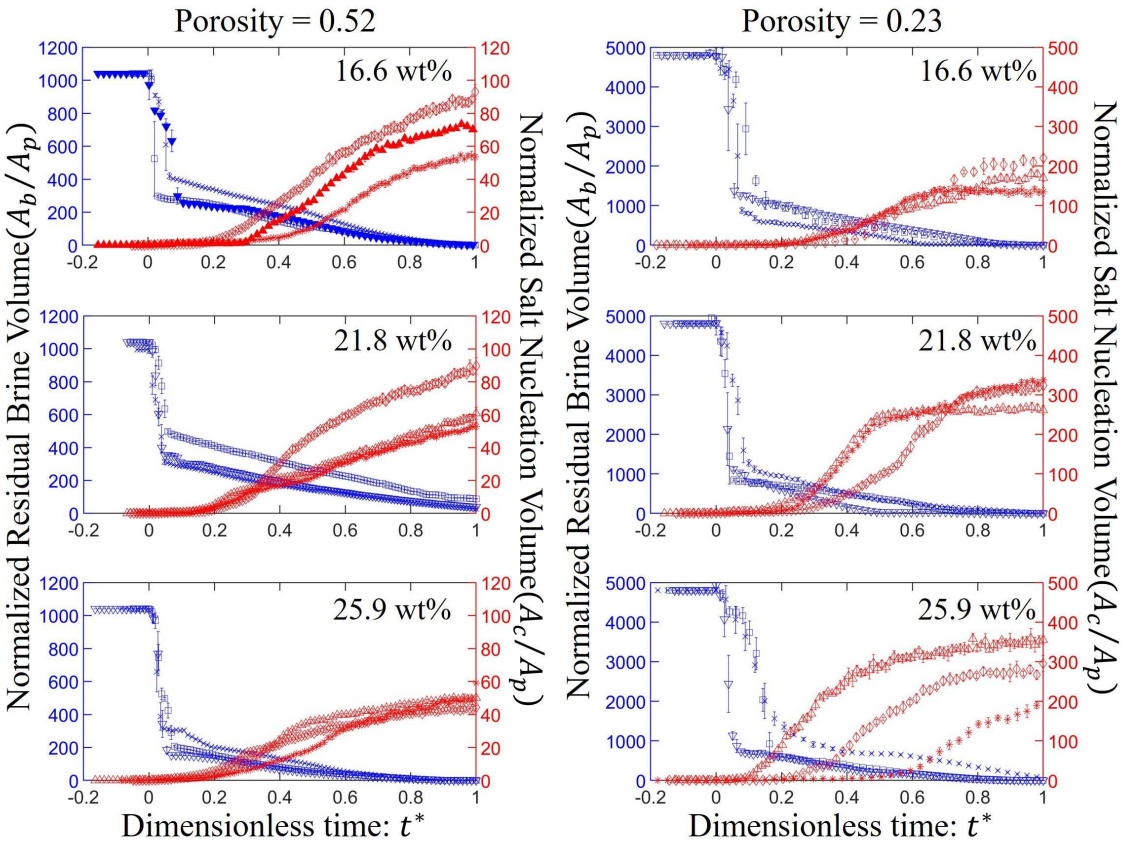

FIG. S5 The data summary of brine evaporation (shown by □, ▽, and ×) and salt growing (indicated by ◇, △, and ⋆) rates varying with dimensionless time in this experimental study. The two columns show the two different porosity cases, and the initial salt concentration increases from the first row (16.6 wt%) to the third row (25.9 wt%). The representative data for Fig. 2 (b) in the paper is highlighted by the solid triangles (▼ and ▲) for $\phi = 0.52$ and 16.6 wt% salt-concentration.

[1] S. Weides, I. Moeck, J. Majorowicz, and M. Grobe, Canadian Journal of Earth Sciences **51**, 783 (2014).

[2] P. H. Nelson, AAPG bulletin **93**, 329 (2009).

[3] R. Legtenberg, H. Jansen, M. De Boer, and M. Elwenspoek, J. Electrochem. Soc. **142**, 2020 (1995).

[4] D. Qin, Y. Xia, and G. M. Whitesides, Nat. Protoc. **5**, 491 (2010).

[5] T. Ferreira and W. Rasband, ImageJ/Fiji **1**, 155 (2012).

[6] A. Sharma, *Understanding color management* (John Wiley & Sons, 2018).